# A CT Saturation Detection Algorithm Using Symmetrical Components for Current Differential Protection

Nicholas Villamagna and Peter A. Crossley, *Member, IEEE*

***Abstract*—A method of symmetrical component analysis for the detection of current-transformer (CT) saturation in a numerical current differential feeder protection relay is presented in this paper. The performance of the differential relay is investigated for various faults on a typical Electro-Magnetic Transients Program/Alternative Transients Program (EMTP/ATP) simulated transmission feeder. The simulator includes the effects of CT saturation. A comparison between simulation and tests conducted on an analog model testbench are also evaluated. The results show a high degree of similarity and illustrate the effect that CT saturation imposes on the sensitivity and stability of the protection scheme. An algorithm is presented that shows significant improvement in sensitivity on internal faults while still maintaining a high level of stability on external faults and nonfault events.**

***Index Terms*—Current-transformer (CT) saturation, gradient, hysteresis data (HYSDAT), rate of change, sliding data window, symmetrical component, testbench.**

## I. Introduction

THE BASIC operating principle of current differential protection is to calculate the difference between the current entering and leaving the protected zone. The simplicity of comparing the current flowing into a feeder with the current flowing out is very attractive, particularly when one considers the complexities of setting a distance protection scheme. It is inherently selective, allowing for sensitive detection of internal faults, while ignoring other events such as external faults, load current, and power swings. Another important benefit is that simultaneous tripping at both transmission-line terminals can be affected, irrespective of the relative current contribution from the sources at both ends.

The protection operates when the differential current exceeds a set bias threshold. For external faults, the differential current should be zero, but errors caused by CT saturation can result in a nonzero value. To ensure stability (i.e., to prevent maloperation, the operating threshold is raised by increasing the bias setting). This prevents maloperation by raising the setting of the relays in proportion to the magnitude of the throughfault current. Enhanced stability is ensured by increasing the bias threshold at the expense of protection sensitivity. Raising the bias threshold has a detrimental effect on the relay sensitivity as it prevents the detection of in-zone resistive faults.

When considering a protection CT, the flux density required to drive the normal load current and low values of fault current through the relays connected to the CT are normally well within the linear region of the B-H curve [1]. Consequently, the excitation current is small and the secondary current is the ratio replica of the primary current. However, if the fault current is high and contains a dc offset, then unless a large over-dimensional CT has been selected, the flux in the core will enter the saturated region of the B-H curve. During the period when the flux is within this region, the excitation current will be high and the secondary current will be severely distorted.

Saturation of a CT resulting from a high current in-zone fault is unlikely to affect the operation of the differential protection. The magnitude of the differential current will be reduced but it will still exceed the bias threshold by a considerable margin. The concerning problem caused by an in-zone fault is the effect on the future stability of the protection, due to the remanent flux left in the CT after the in-zone fault has been cleared. Since the load current is unlikely to reduce the remanent flux to a low value, the flux in the core will continue to cycle around the remanent value, creating a minor B-H loop. This will continue until the next high-current fault occurs. Then, depending on the point on wave (POW) at which a fault occurs, the remanent flux in the core may either increase, driving the CT into deeper saturation, or decrease, reducing or eliminating the level of saturation. The former case may cause a major problem for a differential protection relay if a second fault occurs outside the protected zone (external fault) and one of the CTs has a high value of remanent flux. In this case, the differential current should be zero, but it will no longer be a zero value and may exceed the bias threshold, causing the differential protection to maloperate. In practice, stability is maintained even when an external fault occurs by raising the bias threshold or by selecting a large over-dimensional CT that avoids saturation. The former decreases protection sensitivity, while the latter is not cost effective. Other techniques [2], [3] describe how a saturation detection algorithm can be applied to transmission feeders protected by a differential protection scheme. These techniques along with the proposed algorithm provide alternative means in coping with CT saturation (i.e., maintaining system stability without hindering the sensitivity of the differential protection scheme).

The general concept of symmetrical components was first developed by Fortescue in 1918 [4]. He introduced them for the

Manuscript received February 26, 2004; revised June 17, 2004. This work was supported in part by the U.K. Engineering and Physical Science Research Council, in part by the National Grid Company, in part by Scottish Power, in part by Hathaway Corporation, and VATECH Reyrolle. Paper no. TPWRD-00081-2004.

The authors are with The School of Electrical and Electronic Engineering, Queen's University of Belfast, Belfast BT9 5AH, U.K. (e-mail: n.villamagna@ee.qub.ac.uk; p.crossley@ee.qub.ac.uk).

Digital Object Identifier 10.1109/TPWRD.2005.848654

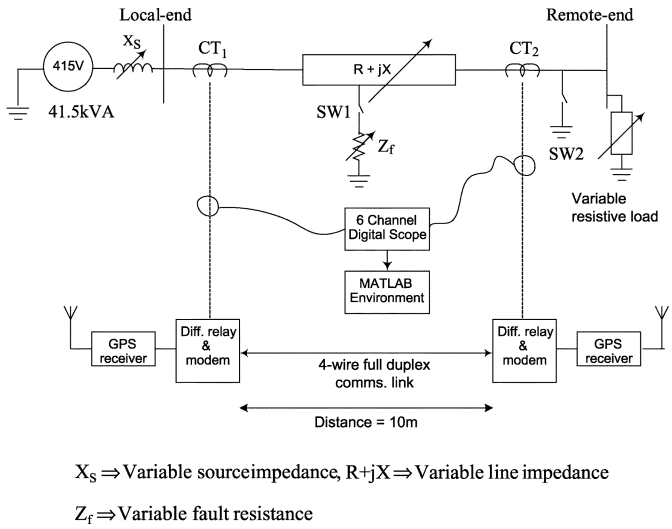


Fig. 1. The 415-V transmission-line testbench.

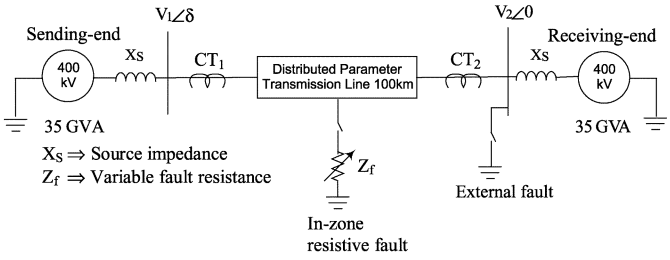


Fig. 2. The 400-kV EMTP system model.

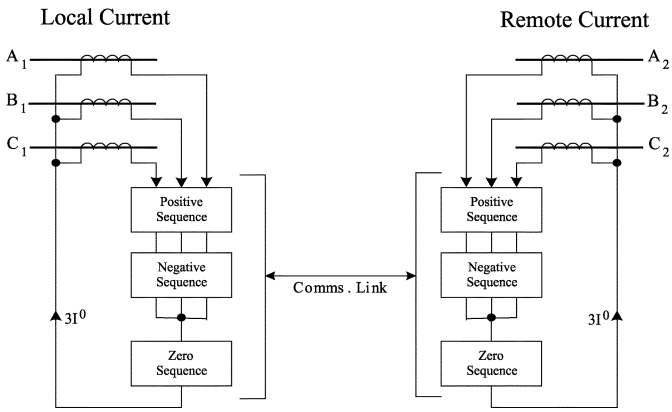


Fig. 3. Symmetrical component evaluation within a current differential relay.

decomposition of complex steady-state phasors. Symmetrical components allow any unsymmetrical set of three-phase currents (or voltages) to be expressed as the phasor sum of three symmetrical ac current (or voltage) components. The symmetrical component transformation matrix is given by (1)

$$\begin{bmatrix} \mathrm{I}^0 \\ \mathrm{I}^1 \\ \mathrm{I}^2 \end{bmatrix} = \frac{1}{3} \begin{bmatrix} 1 & 1 & 1 \\ 1 & \mathrm{a} & \mathrm{a}^2 \\ 1 & \mathrm{a}^2 & \mathrm{a} \end{bmatrix} \begin{bmatrix} \mathrm{I_a} \\ \mathrm{I_b} \\ \mathrm{I_c} \end{bmatrix} \tag{1}$$

where $\mathrm{a} = e^{j(2\pi/3)}$.

Symmetrical components is a powerful tool for the analytical treatment of asymmetrical conditions in a three-phase system. The proposed algorithm computes the positive-sequence (+ve sequence), negative-sequence (−ve sequence), and zero-sequence components of the differential current and also monitors the rate of change of the sequence component currents.

Under normal operating conditions, the current phasors on a transmission feeder are approximately symmetrically balanced and become significantly unbalanced when an asymmetrical fault occurs. Under normal operating conditions or during a three-phase fault (LLL), the behavior of the feeder is determined using only the +ve sequence current. For interphase faults clear of ground (LL), +ve and −ve sequence currents occur and for single-line and double-line-to-ground faults (SLG and LLG), all of the three sequence currents exist.

Transformation of the differential current from the phase domain to the sequence component domain allows the differential protection scheme to more sensitively detect the system changing from a symmetrical condition to an asymmetrical fault condition. Applying this concept to detect CT saturation gives an early indication of a CT being driven into saturation.

## II. System Model

Fig. 1 describes the structure of an analog relay testbench protected by a global positioning system (GPS) synchronized current differential relaying scheme. The analog 415-V three-phase testbench is configured to represent a single-end-fed two-terminal transmission line. The testbench allows for in-zone and external faults to be applied. SW1 is closed to apply an in-zone fault and SW2 is closed for an external fault. The type of fault is determined by a user-selectable switch (i.e., LLL, LL, SLG, and LLG). The line and source reactance and resistance can also be set by the user.

From Fig. 1, the output current signals, from the real CTs, are captured by a six-channel digital oscilloscope. The discrete data are then transported to MATLAB for processing.

Fig. 2 is the Electro-Magnetic Transients Program (EMTP) power system network model configured to represent a typical U.K. 400-kV interconnected power system in which power can flow in either direction.

The system model is a 100-km transmission feeder with six CT models [5]–three at the sending end and three at the receiving end. The generated data are then transported to MATLAB for processing. The EMTP CT model is described in Section III. The physical implementation of the current differential protection is described in Fig. 3.

Fig. 4 describes the functional elements in the current differential relay model implemented using MATLAB. The relay model is described in Section IV.

## III. EMTP CT Model

The transient response of CTs and the correct models in an EMTP simulation are very important in the evaluation of high-speed relaying systems [6]. The model is especially important for studying CT saturation, harmonics, and their affect on the performance of the protective relay. The model allows the user to represent the effects of residual flux left in the CT after interruption of a previous fault.

The hysteresis effects in the CT were modeled in EMTP using the Type-96 nonlinear element and the auxiliary program HYSDAT [5]. HYSDAT automatically generates a hysteresis

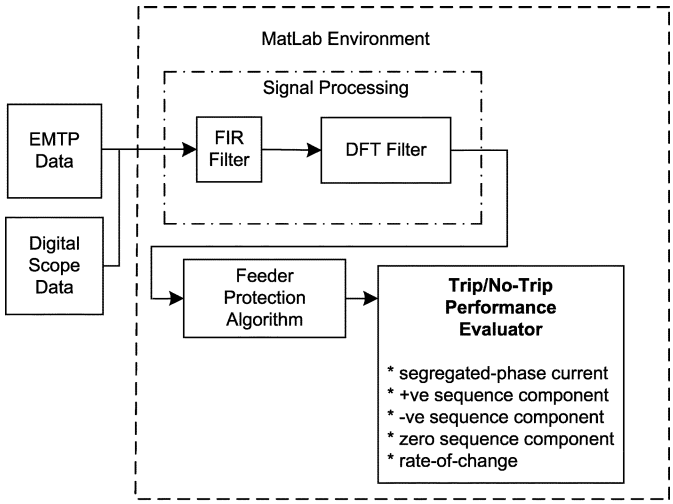


Fig. 4. MATLAB relay model.

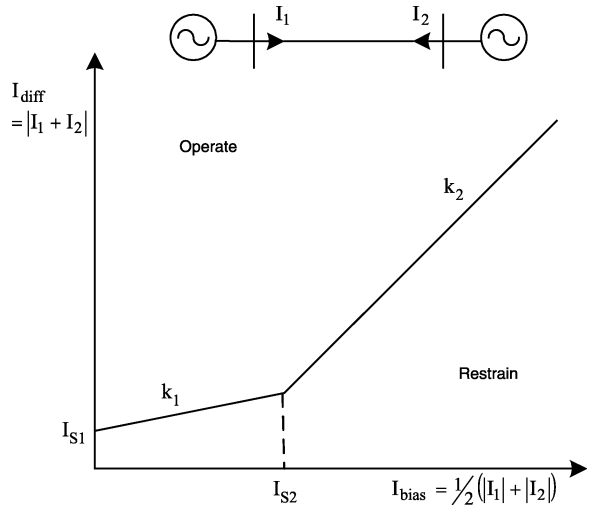


Fig. 5. Dual bias current differential characteristic.

loop when the saturation point (flux current: $(\lambda - i)$) is specified. This routine contains predefined trajectories in the $\lambda - i$ plane to decide which path to follow when the flux increases or decreases. The shape of the loop is a function of the core material and the geometry [7]. EMTP supports one type of material; the ARMCO M4-oriented steel. The CT knee-point voltage $(V_k)$ is given by (2)

$$V_k = 4.44 f \lambda \tag{2}$$

where $V_k$ is the root mean square (rms) knee-point voltage, $f$ is the system frequency, and $\lambda$ is the instantaneous flux. Since the model parameters are derived from CT test data, a degree of validity is implied [6].

## IV. Relay Model

A current differential relay was developed within MATLAB [8]. The algorithm applied in MATLAB consists of a finite-impulse-response (FIR) lowpass filter, a discrete Fourier transform (DFT) routine, and a model that implements a segregated-phase dual slope percentage bias current differential protection scheme [9]. The operating characteristic of the dual slope, biased current differential element for a two-terminal feeder is shown in Fig. 5. The dual slope restraint characteristic is a form of adaptive restraint in which the magnitude of the restraint quantity is increased for high-current conditions where CT saturation becomes more probable.

The operating criteria is described by (3) and (4)

$$\mathrm{I_{op}} = |\mathrm{I_{diff}}| \geq \mathrm{k_1}|\mathrm{I_{bias}}| + \mathrm{I_{s1}} \tag{3}$$

$$\mathrm{I_{op}} = |\mathrm{I_{diff}}| \geq \mathrm{k_2}|\mathrm{I_{bias}}| - (\mathrm{k_2} - \mathrm{k_1})\mathrm{I_{s2}} + \mathrm{I_{s1}} \tag{4}$$

where $\mathrm{I_{op}}$ is the relay operating current. Equation (3) is applied when $|\mathrm{I_{bias}}| \leq \mathrm{I_{S2}}$ and (4) when $|\mathrm{I_{bias}}| \geq \mathrm{I_{S2}}$. The sensitivity setting of $\mathrm{I_{S1}}$ and $\mathrm{k_1}$ in (3) is an important factor for the differential relay because it is more susceptible to fixed errors, such as charging current and CT errors when $\mathrm{I_{bias}} \leq \mathrm{I_{S2}}$ [10].

The FIR filter and the DFT routine process the input data and extract the power frequency current phasors at a sampling rate of 6400 samples/s (128 samples/cycle). The Fourier routine employs a sliding 20-ms data window that calculates a new 50-Hz phasor every $2 \cdot 5$ ms.

## V. CT Saturation Algorithm

The proposed algorithm monitors only the zero-sequence component of the differential current for detecting CT saturation. For every $2 \cdot 5$-ms shift in the DFT data window, the rate of change of the zero-sequence differential current component $(di^0_{\mathrm{diff}}/di_{\mathrm{bias}})$ is computed by (5)

$$m^0_{\mathrm{diff}} = \frac{I^0_{\mathrm{diff}}(n-1) - I^0_{=\mathrm{diff}}(n)}{I_{\mathrm{bias}}(n-1) - I_{\mathrm{bias}}(n)} \tag{5}$$

where $m^0_{\mathrm{diff}}$ is the zero-sequence differential current gradient with respect to the bias current. $I^0_{\mathrm{diff}}(n)$ is the initial (1st) zero-sequence differential current value computed with $n = 0$ relating to the first DFT sliding data window and $I_{\mathrm{bias}}(n)$ is the initial phase domain bias current evaluated. The instant of a significant rate of change [3] of differential current clearly marks the start of CT saturation. The polarity of the gradient $(m^0_{\mathrm{diff}})$ distinguishes an in-zone fault from an external fault (see results, Section VI and VII). For an external fault involving CT saturation, a "positive" significant rate-of-change value $(m^0_{\mathrm{diff}} = +\mathrm{ve\ value})$ is classified as an external fault. For a "negative" gradient value, an in-zone fault is classified.

When a CT is driven into saturation, the third harmonic is largely responsible for the sharp peak in the waveform of the CT current [11] (Fig. 9). By Fourier series expansion, [12] describes how all triplen harmonics are entirely zero sequence. That is, the similarity between the third harmonic component and the fundamental zero-sequence component is that they are both cophasal. Therefore, since CT saturation always produces a third harmonic component, a zero-sequence component will always be present in the differential current signal from a set of saturated CTs. This is irrespective of whether the fault involves a ground path. Therefore, for a LL fault clear of ground, the algorithm is able to detect the zero-sequence current component if a CT is driven into saturation. Where in [3], the phase domain rate of change of differential current is monitored, the proposed

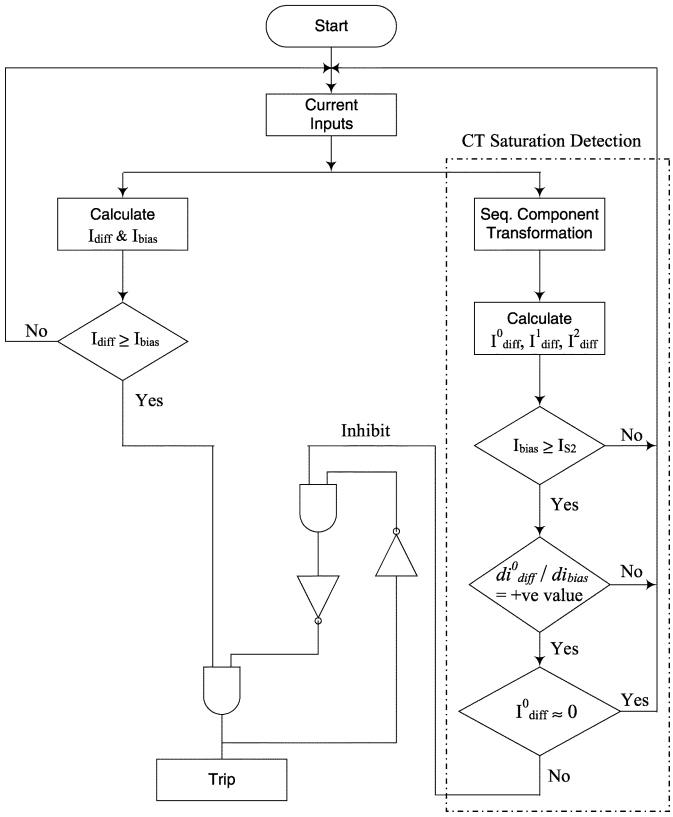


Fig. 6. Current differential relay flowchart.

algorithm enhances sensitivity by monitoring the zero-sequence differential current component to detect CT saturation.

The flowchart of the proposed algorithm describing CT saturation detection is depicted as Fig. 6. The sequence domain transformation as described by (1) computes the +ve sequence, −ve sequence and zero-sequence differential current. Detection of CT saturation is only initiated when the bias current is greater than or equal to $I_{S2}$, (i.e., $I_{bias} \geq I_{S2}$) (Fig. 5) (i.e., where the threshold setting is determined by the $k_2$ slope). The $k_2$ slope is the higher percentage bias setting designed to improve relay stability against CT saturation under heavy throughfault current (external fault) conditions [13]. With $I_{S2} = 2 \cdot 0$ p.u., this ensures that detection of CT saturation is only applied under heavy throughfault current conditions (external faults), where the relay operates when $I_{bias} \geq I_{S2}$ as described in (4).

Once the bias current is within the region of the $k_2$ slope threshold (i.e., $I_{bias} \geq I_{S2}$) and a positive rate-of-change value in the zero-sequence differential current is detected (Figs. 8, 12, and 14) and as given by (5), an inhibit signal prevents the relay from initiating a "trip" command. The CT saturation detection is then reset (i.e., released) once the magnitude of the zero-sequence differential current is approximately equal to zero ($|I^0_{diff}| \approx 0$). This ensures that the CT is no longer operating in a saturated condition.

## VI. Testbench Results

For the analog model power system (testbench), the CTs measure the primary current signals caused by a short-circuit fault. All tests conducted on the testbench are SLG ($A\phi - G$) faults

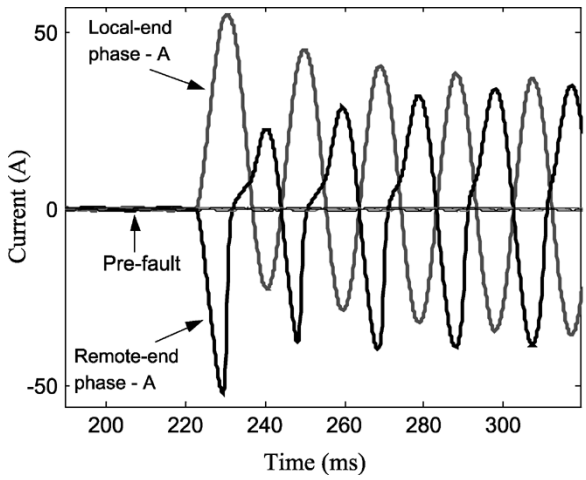


Fig. 7. Testbench SLG ($A\phi - G$) external fault.

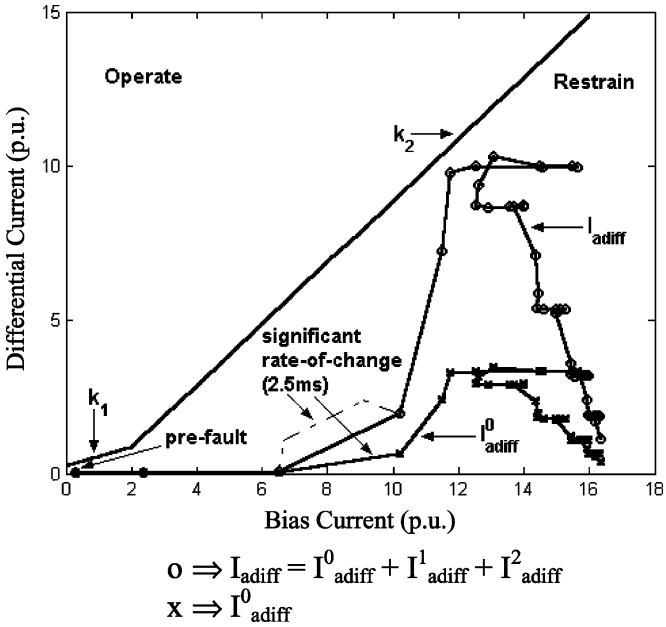


Fig. 8. Phase-A differential current loci: external fault.

with a balanced prefault load current. For external faults, an X/R ratio of 40 was chosen, emulating the power system time constant seen by the CTs for a fault at the source. The ratio for both sets of CTs was selected as 1:1. A CT burden was selected to cause deep saturation (dependent on the point-on-wave of the fault). A number of tests were conducted in order to capture a range of CT saturation levels (arbitrary point-on-wave switching). The result chosen is one of the more severe cases of CT saturation.

Fig. 7 is the CT current for a SLG ($A\phi - G$) external fault. At the maximum dc offset, the phase-A CT current at the remote end of the protected zone is driven into saturation for approximately 100 ms.

Fig. 8 describes the phase-A differential current verses bias current characteristic. The parameter settings for the dual bias slope are $I_{S1} = 0.25$ p.u., $I_{S2} = 2.0$ p.u., $k_1 = 30\%$, $k_2 = 100\%$.

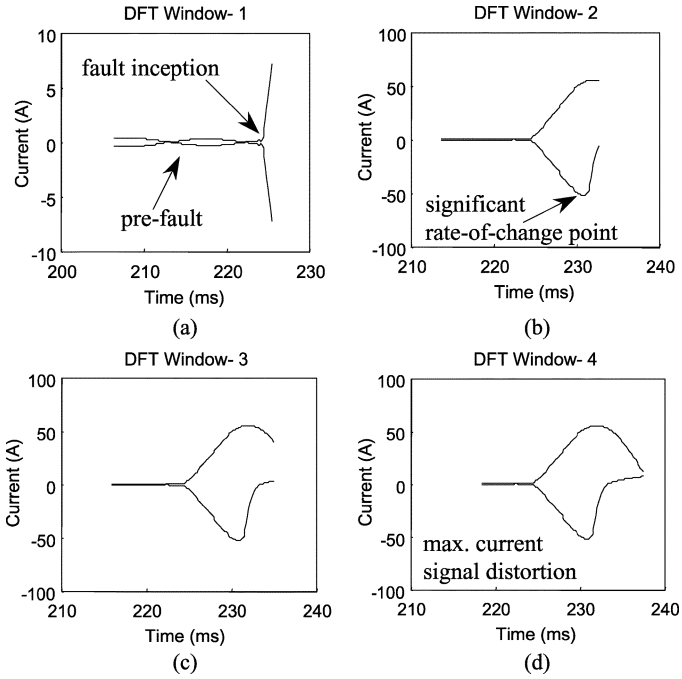


Fig. 9. Local and remote-end phase–a DFT data window.

Each consecutive point (i.e., "o" and "x") marks a $2 \cdot 5$-ms shift in the DFT sliding data window. The "o" points mark the locus of the phase-A differential current $(\mathrm{I_{adiff}})$ and "x" is the zero-sequence differential current $(\mathrm{I^0_{adiff}})$. Note: $\mathrm{I_{adiff}}$ is the total phase current component, equal to the summation of the $+\mathrm{ve}(\mathrm{I^1_{adiff}})$, $-\mathrm{ve}(\mathrm{I^2_{adiff}})$, and zero $(\mathrm{I^0_{adiff}})$ sequence differential currents. Fig. 8 shows that immediately after fault inception, there is an increase in bias current with no appreciative increase in differential current (i.e., the horizontal trajectory moving from $\mathrm{I_{bias}} = 0 \cdot 3 \rightarrow 6 \cdot 5$ p.u.). The point of the "significant rate of change" $(di_{\mathrm{adiff}}/di_{\mathrm{abias}})$ and $(di^0_{\mathrm{adiff}}/di_{\mathrm{abias}})$ marks the start of the current distortion caused by the saturation of the CT core. From this point, a rapid increase in differential current is noticed. Both $\mathrm{I_{adiff}}$ and $\mathrm{I^0_{adiff}}$ have the same locus trajectory, with $\mathrm{I^0_{adiff}}$ being approximately one-third of the magnitude of $\mathrm{I_{adiff}}$. This is as expected since the fault is $\mathrm{A}\phi - \mathrm{G}$ and $\mathrm{I^0_a} = \mathrm{I_A}/3$. Also note that the significant rate of change commences when $\mathrm{I_{bias}} = 6 \cdot 5$ p.u. This agrees with $\mathrm{I_{bias}} \geq \mathrm{I_{S2}}$ $(\mathrm{I_{S2}} = 2.0$ p.u.), where CT saturation becomes more probable due to a heavy throughfault current (external fault). The CT saturation detection is initiated once the bias current exceeds the $\mathrm{I_{S2}}$ setting and then begins to monitor the rate of change of the zero-sequence differential current (Fig. 6).

Fig. 9 shows the DFT sliding data windows of the phase-A current signal. Each data window marks a $2 \cdot 5$-ms shift.

Fig. 9(a) shows that at the point of fault inception, the local and remote-end current rapidly increases and there is no distortion in the current signals. This is seen in Fig. 8, where the trajectory shows an increase in bias current (i.e., throughfault current) with no developed differential current. Fig. 9(b) corresponds to the next shift of DFT data window. The window captures the start of the distortion in the remote-end current. At this point, a significant rate of change in differential current is developed. This is seen in Fig. 8 as the first initial rise in the differential

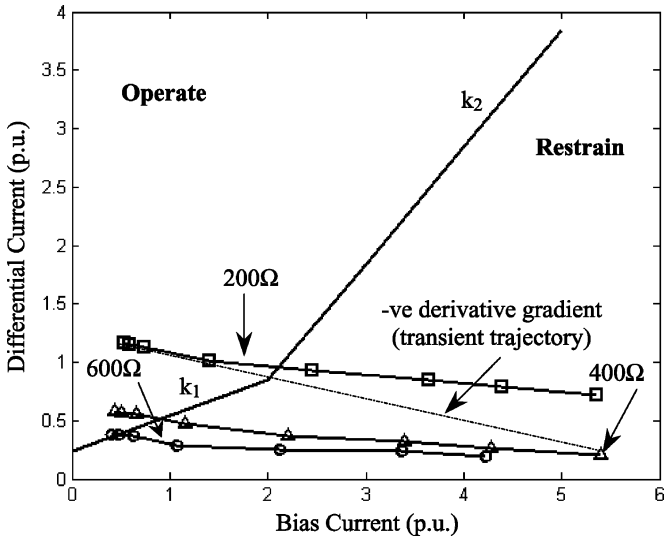


Fig. 10. In-zone SLG $(\mathrm{A}\phi - \mathrm{G})$ resistive fault.

current trajectories of both $\mathrm{I_{adiff}}$ and $\mathrm{I^0_{adiff}}$. That is, a significant rate of change in both $di_{\mathrm{adiff}}/di_{\mathrm{abias}}$ and $di^0_{\mathrm{adiff}}/di_{\mathrm{abias}}$ is noticed and where by applying (5), $\mathrm{m^0_{adiff}} = +\mathrm{ve}$ value.

For in-zone resistive fault tests, an X/R ratio of 16 was chosen. This is the typical value for a 400-kV transmission line in the U.K. The in-zone resistive faults were applied at the midpoint of the transmission line with all CTs operating in ideal conditions (i.e., CTs operating in the linear region of the B-H curve). Fig. 10 shows how the differential current $(\mathrm{I_{adiff}})$ loci change as the through load current is increased. From Fig. 10, it can be seen that an increase in through load current results in a reduction in the sensitivity of the relay.

It should be noted that Fig. 8 is a transient trajectory and Fig. 10 is a steady-state trajectory. The "dashed line" ($-$ve derivative slope) in Fig. 10 signifies the transient trajectory as the fault resistance changes. Comparing Fig. 8 with Fig. 10, it can be seen that the significant rate-of-change polarity of $di_{\mathrm{adiff}}/di_{\mathrm{abias}}$ and $di^0_{\mathrm{diff}}/di_{\mathrm{abias}}$ is positive in Fig. 8 and that transient trajectory (denoted by the dashed line), $di_{\mathrm{adiff}}/di_{\mathrm{abias}}$, depicted in Fig. 10 is negative as the in-zone fault resistance changes. A significant rate of change with a positive gradient occurs when CT saturation is caused by a heavy throughfault current (external fault) and a negative gradient occurs for an in-zone fault.

## VII. EMTP Simulation Results

For simulations involving CT saturation, both external and in-zone faults were considered. A transmission-line X/R ratio of 40 was chosen for both cases. To emulate the worse case scenario, the CTs at the receiving end were prevented from being driven into saturation.

The in-zone resistive fault simulations all involve SLG $(\mathrm{A}\phi - \mathrm{G})$ faults, with all of the CTs operating in an unsaturated condition. An X/R ratio of 16 was chosen and all of the faults were applied at the midpoint of the transmission line.

For all of the tests, a CT ratio of 2000:5 with a knee-point voltage of 300 V given by (2) and a resistive burden of $1 \cdot 5\ \Omega$ was chosen.

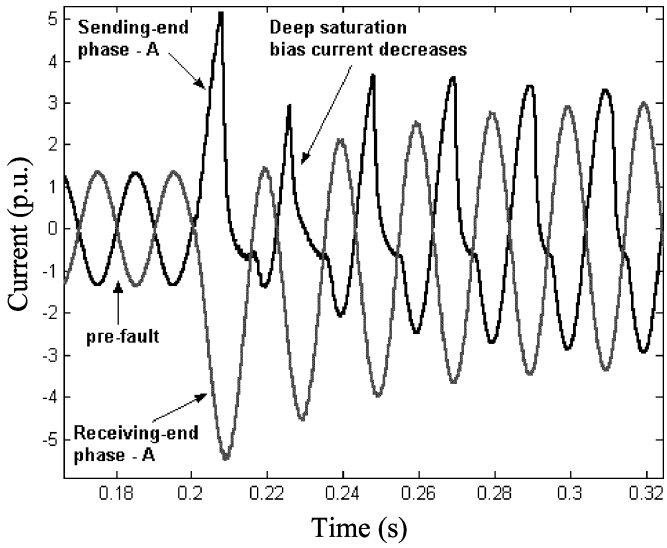


Fig. 11. EMTP: SLG $(\mathrm{A}\phi - \mathrm{G})$ external fault.

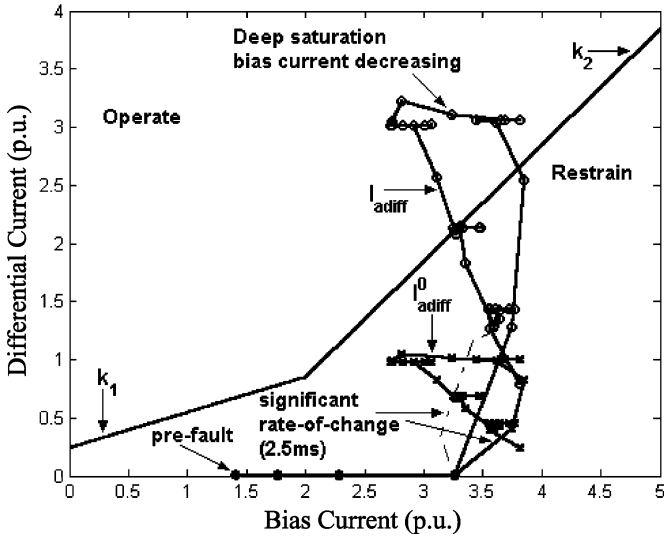


Fig. 12. Phase-A differential current loci: external fault.

Two types of external faults that cause CT saturation were considered: i) SLG $(\mathrm{A}\phi - \mathrm{G})$; and ii) LL $(\mathrm{B}\phi - \mathrm{C}\phi)$ faults. In both cases, the point on wave of fault inception was such as to cause maximum asymmetry in phase-A (for SLG fault) and phase-B (for LL fault).

For the SLG external fault, the phase-A CT at the sending end is driven into saturation half a cycle after fault inception, as shown in Fig. 11. A residual flux of $-80\%$ was selected for the sending-end phase-A CT. All other CTs remained in an unsaturated condition.

Within the second cycle, the CT is driven further into saturation, denoted as "deep saturation." This is depicted in Fig. 12 where the bias current decreases when the differential current increases.

Fig. 12 shows the developed phase-A differential current characteristic due to saturation of the sending-end CT. Note: both $\mathrm{I_{adiff}}$ and $\mathrm{I^0_{adiff}}$ have the same locus trajectory, with $\mathrm{I^0_{adiff}}$ being approximately one-third of the magnitude of $\mathrm{I_{adiff}}$.

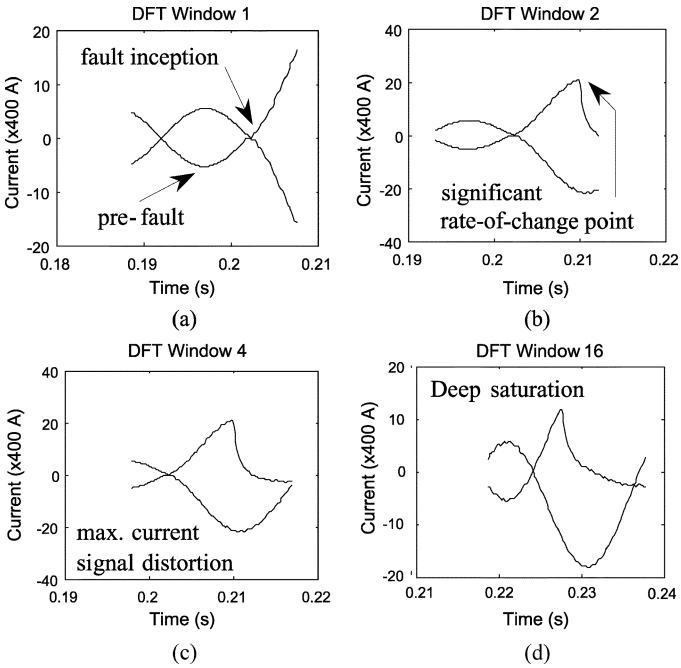


Fig. 13. Sending and receiving-end phase-A DFT data windows.

The DFT window in Fig. 13 captures a section of the first two cycles of CT saturation. Fig. 13(a) captures the prefault and fault inception. Fig. 13(b) is shifted $2 \cdot 5$ ms from the first window, capturing the start of the "significant rate-of-change" point. Fig. 13(c) is shifted $4 \cdot 5$ ms from the first window, capturing the entire first half a cycle showing maximum current distortion. Fig. 13(d) is shifted $37 \cdot 5$ ms (second cycle) from the first window, capturing the "deep saturation" (max. $\mathrm{I_{adiff}}$ and $\mathrm{I^0_{adiff}}$, at min. $\mathrm{I_{abias}}$) cycle. Taking the "numeric area of integration" (i.e., the area under the curve), we see that in Fig. 13(d), the area under the curve is less than in Fig. 13(c). This gives rise to a reduced bias current against a maximum rise in differential current, as seen in Figs. 12 and 14 (denoted "deep saturation").

For the LL $(\mathrm{B}\phi - \mathrm{C}\phi)$ external fault, the phase-B differential current loci are shown. A residual flux of $+80\%$ was chosen for the phase-B sending-end CT. Both the phase-B and phase-C CTs at the sending end were driven into saturation, with all other CTs remaining in the unsaturated state. The differential current loci of phase-B are described in Fig. 14.

Observing Fig. 14(a) and (b), the positive-sequence $(\mathrm{I^1_{bdiff}})$ and the negative-sequence $(\mathrm{I^2_{bdiff}})$ differential current trajectories show close similarities. Fig. 14(c) shows that the zero-sequence differential current $(\mathrm{I^0_{bdiff}})$ trajectory is less than one-third of the magnitude of $\mathrm{I_{bdiff}}$. This is as expected since for the LL fault, the zero-sequence differential current is due only to the predominately large third harmonic component which exists only when the CT is saturated (i.e., it has the same characteristic as the zero-sequence component). In this case, for an LL fault, the zero-sequence differential current is less than the zero-sequence differential current developed for an SLG fault, since there is no ground path. Noting that for an LL fault in which the CT does not saturate, only the positive-sequence and negative-sequence current component exist in which $\mathrm{I^2} = -\mathrm{I^1}$.

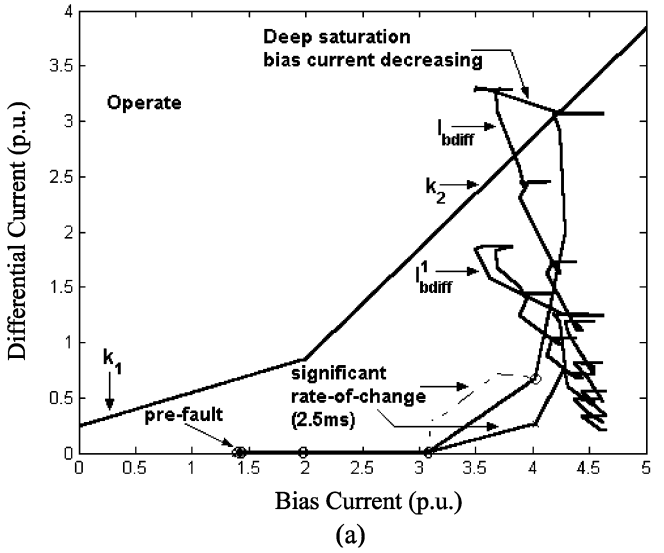


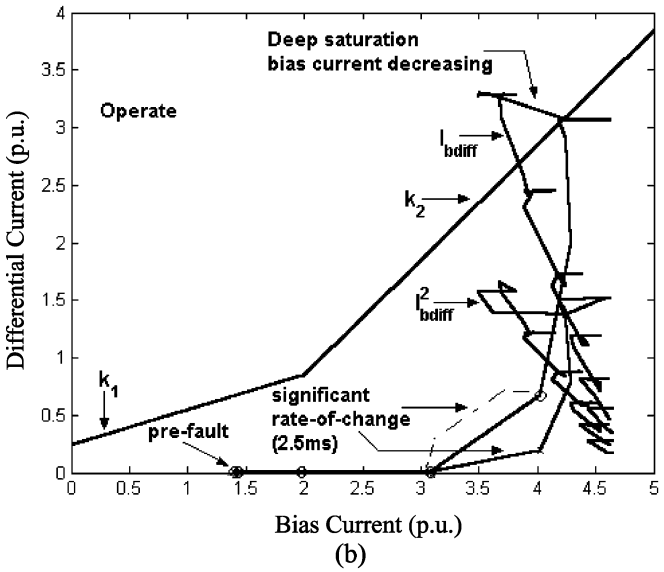


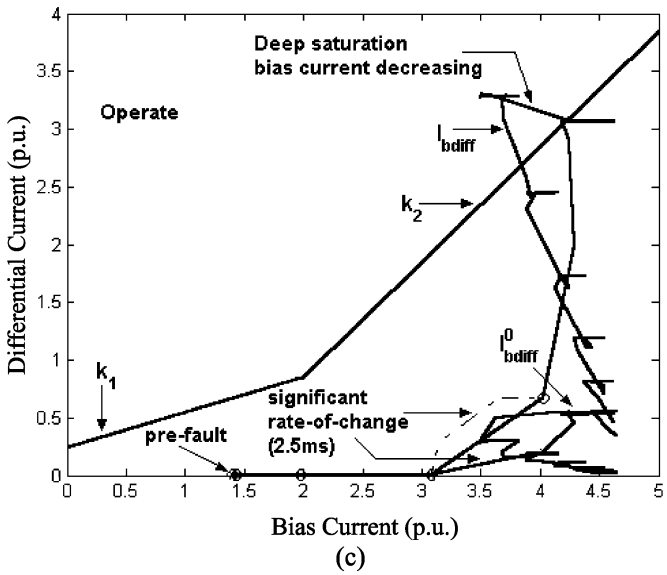


Fig. 14. Phase-B differential current loci: external fault.

Fig. 15 describes the differential current trajectory for an SLG $(\mathrm{A}\phi - \mathrm{G})$ in-zone fault when the phase-A sending-end CT is driven into saturation. A residual flux of $-80\%$ was chosen for the phase-A sending-end CT. All of the other CTs operated in the unsaturated condition.

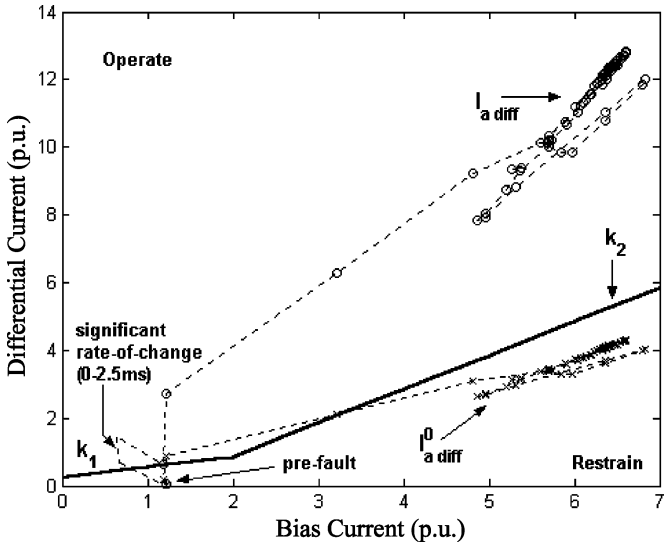


Fig. 15. Phase-A differential current loci: in-zone fault.

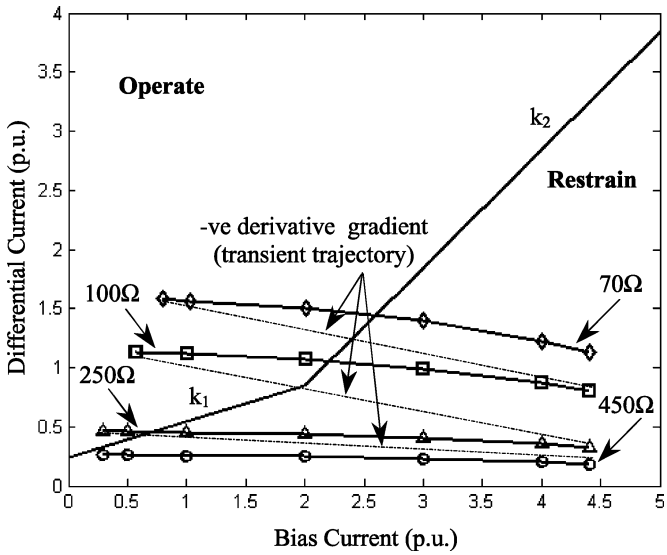


Fig. 16. In-zone SLG $(\mathrm{A}\phi - \mathrm{G})$ resistive fault.

Referring to Fig. 15, the initial significant rate of change of $\mathrm{I_{adiff}}$ and $\mathrm{I^2_{adiff}}$ both lie between a perpendicular gradient from the point of prefault, to a negative gradient. For the perpendicular gradient, the derivative is infinite (i.e., for a tangent at 90°, an infinite value is evaluated). Also noting that at the point of fault inception, there is an immediate rise in differential current and no immediate increase in bias current. This trajectory (Fig. 15) notably differs from the trajectory seen in Fig. 8, Fig. 12, and Fig. 14, which are characteristic to external faults.

Since the bias current at the point of fault inception is less than the $\mathrm{I_{S2}}$ setting (Fig. 15), a "trip" command from the relay can be initiated, (providing it exceeds the $\mathrm{k_1}$ slope threshold) (i.e., the CT saturation detection is bypassed).

Fig. 16 describes the steady-state differential current $(\mathrm{I_{adiff}})$ loci for various resistive in-zone faults against an increase in through load current. The "dashed line" indicates the transient

trajectory (−ve derivative) of the differential current (i.e., as the fault resistance value changes during the fault period).

Both Fig. 10 and 16 show the situation of how the relay is desensitized as the through load current increases. This compromise between maintaining system stability and relay sensitivity is mainly related to the probability of the CT/CTs, being driven into saturation during a heavy throughfault current condition.

## VIII. Summary

The major conclusion of this study is that the proposed algorithm allows for a differential relay to improve its' ability to be more sensitive while still maintaining the high level of protection stability. Due to the probability of CT saturation occurring during a heavy throughfault condition, the $k_2$ slope in (4) is used to enhance protection stability when $I_{bias} \geq I_{S2}$, but at the expense of reduced protection sensitivity. By monitoring the zero-sequence differential current, the results presented show that the $k_2$ slope can be appreciably reduced or reshaped to provide increased sensitivity while still maintaining the high level of stability. This is achieved by having bias threshold characteristics in (4), sensitive to the zero-sequence differential current for when $I_{bias} \geq I_{S2}$. This also covers LL faults clear of a ground path, where results have shown that when the CT saturates owing to LL faults, a zero-sequence differential current can be detected due to the third harmonic current component.

The results obtained from the analog testbench with those from the simulation tests have shown a high degree of similarity. This confirms that for any further investigation, simulations in EMTP will give realistic results.

## References


[1] P. A. Crossley, H. Y. Li, and A. D. Parker, "Design and evaluation of a current differential relay test system," *IEEE Trans. Power Del.*, vol. 13, no. 2, pp. 427–433, Apr. 1998.

[2] Y. C. Kang, S. H. Ok, and S. H. Kang, "A CT saturation detection algorithm," in *Proc. PowerTech*, Bologna, Italy, 2003.

[3] SEG, Differential Protection Relay for Generators and Motors, Model IRD1-G, Tech. Manu.

[4] C. L. Fortescue, "Method of symmetrical coordinates applied to the solution of polyphase networks," *Trans. AIEE*, vol. 37, pp. 1027–1140, 1918.

[5] EPRI, Electromagnetic Transients Program (EMTP), Version 1, Revised Rule Book, Vancouver, CA, vol. 1, Apr. 1986.

[6] D. A. Tziouvaras and P. McLean *et al.*, "Mathematical models for current, voltage and coupling capacitor voltage transformers," *IEEE Trans. Power Del.*, vol. 15, no. 1, pp. 62–72, Jan. 2000.

[7] M. Kezunovic and L. Kojovic *et al.*, "Experimental evaluation of EMTP-based current transformer models for protective relay transient study," *IEEE Trans. Power Del.*, vol. 9, no. 1, pp. 405–413, Jan. 1994.

[8] N. Villamagna, P. A. Crossley, and H. Y. Li, "GPS synchronized current differential protection with adaptive bias operating characteristic," in *Proc. Int. Symp. Modern Electric Power Systems*, Wroclaw, Poland, 2002.

[9] H. Ito and I. Shuto *et al.*, "Development of an improved multifunctional transmission line protection," in *Developments in Power System Protection*, 2001, Conf. Pub. 479.

[10] M. Yamaura, Y. Kurosawa, and H. Ayakawa, "Improvement of internal charging current compensation for transmission line differential protection," in *Proc. Developments Power System Protection*, 1997, Conf. Pub. 434.

[11] Members of the staff of Dept. Elect. Eng., Massachusetts Inst. Technol., *Magnetic Circuits and Transformers*. New York: Wiley, 1946, pp. 173–184.

[12] G. J. Wakileh, *Power Systems Harmonics—Fundamentals, Analysis and Filter Design*. Berlin, Germany: Springer, 2001, pp. 13–15.

[13] GEC ALSTOM, Digital Current Differential Relay—Type: LFCB 102, Techn. Manu.



**Nicholas Villamagna** received the Electrical Fitting (Electrical Technician) diploma from the Fremantle Technical College, Perth, Western Australia, in 1986. He received the B.Eng. (Hons.) degree in electrical engineering from Brunel University, Brunel, U.K., in 1998 and the M.Sc. degree in electrical power systems from the University of Manchester Institute of Science and Technology, Manchester, U.K., in 2000. He is currently pursuing the Ph.D. degree in power system protection at Queen's University of Belfast, Belfast, U.K.

He was in industry for 13 years, specializing in machines and control systems.

**Peter A. Crossley** (M'96) received the B.Sc. degree from the University of Manchester Institute of Science and Technology (UMIST), Manchester, U.K., in 1977 and the Ph.D. degree from the University of Cambridge, Cambridge, U.K., in 1983.

Currently, he is Professor of Electrical Engineering at Queen's University of Belfast, Belfast, U.K. He had been involved in the design and application of digital protection relays and systems for 25 years, first with GEC, then with ALSTOM, UMIST, and later with Queen's University of Belfast, Belfast, U.K. He has published many technical papers on protection.

Dr. Crossley was the Chairman of the 2001 IEE Development in Power System Protection Conference in Amsterdam, The Netherlands, and is an active member of various CIGRE, IEEE, and Institution of Electrical Engineering committees on protection.